BEILSTEIN JOURNAL OF ORGANIC CHEMISTRY

Intramolecular interactions governing the conformational behavior of 2-aminopropan-1-ol and its methyl ether: hydrogen bonding, gauche effect, and metallic interactions

Lauane C. Mendonça and Matheus P. Freitas*

Full Research Paper

Open Access

Address:
Department of Chemistry, Institute of Natural Sciences, Federal University of Lavras, 37200-900, Lavras, MG, Brazil

Email:
Matheus P. Freitas* - matheus@ufla.br

* Corresponding author

Keywords:
chelation; conformational analysis; gauche effect; hydrogen bonding; hyperconjugation

Beilstein J. Org. Chem. **2026,** *22,* 1649–1659.
https://doi.org/10.3762/bjoc.22.133

Received: 02 September 2026
Accepted: 02 November 2026
Published: 12 November 2026

Associate Editor: P. Schreiner

© 2026 Mendonça and Freitas; licensee Beilstein-Institut.
License and terms: see end of document.

Abstract

Understanding the conformations of amino alcohols is crucial for their applications in fields such as medicinal chemistry and environmental science. Therefore, the conformational analysis of 2-aminopropan-1-ol (**1**) and its methyl ether **2** was performed both quantum-chemically and experimentally, using infrared and NMR spectroscopies. The conformational equilibrium of **1** is primarily governed by an N···H–O intramolecular hydrogen bond. In contrast, its methyl ether derivative lacks this hydrogen-bonding capability and has negligible O···H–N interactions, thus the gauche effect driven by antiperiplanar hyperconjugative interactions dictates its conformational balance. Our study reveals that both types of intramolecular interactions are overridden upon coordination to Zn^{2+} and Cd^{2+} ions. These findings suggest that intramolecular interactions in **1** and **2** are insufficient to prevent chelation with these cations in various systems. This research provides insights into the behavior of these compounds in complex systems and their potential applications in heavy metal remediation.

Introduction

2-Aminopropan-1-ol (**1**) exhibits competitive intramolecular hydrogen bonding, where either the NH_2 or OH groups can act as proton donors. Nitrogen is known to be a superior proton acceptor, likely influencing both the gauche preference and the orientation of hydrogens bonded to heteroatoms in the conformational equilibrium of vicinal OH and NH_2 groups within an ethane fragment [1,2]. Interestingly, the occurrence of hydrogen bonding involving the OH group and the halogen atom in 2-chloro- and 2-bromopropanol remains controversial, with different studies reaching opposing conclusions [3,4]. Whereas one study reported no significant OH···Cl and OH···Br hydrogen bonding in these compounds [3], another provided evidence for such interactions [4]. This contrasts with the case of 2-iodoethanol, for which an OH···I interaction has also been re-

ported [5]. This raises the question of whether hydrogen bonding dictates the conformational equilibrium in compound **1**, and whether it persists when competing with chelating metals such as Zn^{2+} and Cd^{2+}. Furthermore, although N···H–O intramolecular hydrogen bonding is well documented in amino alcohols [6-10], a direct comparison with the corresponding methyl ethers has received comparatively little attention. Such a comparison could help disentangle the role of hydrogen bonding from other stereoelectronic and conformational effects.

Amino and hydroxy groups are commonly present in bioactive compounds, and despite intermolecular interactions typically prevailing over intramolecular ones [11], such as in enzyme targets, intramolecular hydrogen bonding still persists in the bioconformation of certain ligand compounds [12]. Nonetheless, certain enzymes harbor ions as key entities within or adjacent to a binding site, for instance, zinc metalloenzymes [13]. Zinc in proteins can either directly participate in chemical catalysis or play a crucial role in maintaining protein structure and stability. In all catalytic sites, the zinc ion functions as a Lewis acid and can therefore interact with amino and hydroxy groups of a compound, potentially inducing a conformational change, at least by rotating the C–N and/or the C–O bonds of the substrate. Additionally, the zinc cation forms complexes with electron donors, such as EDTA (ethylenediaminetetraacetic acid), DTPA (diethylenetriaminepentaacetic acid), and citric acid, facilitating its removal from living systems and soil [14,15].

This study aimed to investigate the conformational isomerism of 2-aminopropan-1-ol and its methyl ether, 1-methoxypropan-2-amine (**2**, see Figure 1), with particular emphasis on establishing whether nitrogen is the only proton-donor site available for intramolecular hydrogen bonding. Although aminoethanol would provide a simpler model system, it has already been investigated in previous studies [8,10]. In contrast, 2-aminopropan-1-ol (**1**) has received considerably less attention in this context and offers greater conformational diversity owing to the additional methyl group, thereby providing a broader framework for assessing the role of intramolecular hydrogen bonding in conformational equilibria. Additionally, the influence of Zn^{2+} and Cd^{2+} ions on the conformational equilibria of both compounds was examined. The inclusion of Cd^{2+} is also relevant from an environmental perspective, as Cd is an important soil contaminant whose removal has been investigated using chelating agents such as DTPA [14]. Notably, although Cd^{2+} is not directly coordinated to the carbonyl group in DTPA, a scalar coupling involving Cd and the C(=O) group was experimentally observed, demonstrating that Cd^{2+} coordination can influence scalar couplings transmitted through the molecular framework [14]. Cd^{2+} was therefore selected not only because of its environmental relevance but also because its naturally occurring spin-$^1/_2$ isotopes make it amenable to NMR investigation, providing an experimental complement to the Zn^{2+} system. The investigation combined experimental approaches (infrared spectroscopy and ^3J HH NMR coupling constants involving diastereotopic hydrogens) with theoretical methods, including gas-phase and implicit-solvent optimizations in acetonitrile and natural bond orbital (NBO) analyses.

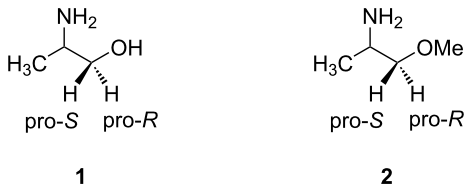


Figure 1: 2-Aminopropan-1-ol (**1**) and its methyl ether **2** studied in this work.

Materials and Methods

Compounds **1** and **2** were commercially available and used without further purification for the infrared and NMR experiments. Infrared spectra were acquired from 0.02 M solutions in $CHCl_3$ and CH_3CN, using a CaF_2 liquid cell with 1 mm optical path length and a Shimadzu Affinity FTIR spectrometer, with 32 scans at 2 cm^{-1} resolution. NMR experiments were conducted on a Bruker 600 MHz spectrometer for ^1H nuclei using 20 mg mL^{-1} solutions in $CDCl_3$ and CD_3CN. $ZnCl_2$ and $CdCl_2$ were added to these solutions until saturation for experiments involving the complexes of compounds **1** and **2**.

Quantum-chemical calculations at the B3LYP-GD3BJ/6-311++G(d,p) level [16-19] were performed for geometry optimizations and frequency calculations of **1** and **2**, both in the gas phase and implicit acetonitrile solution using the solvation model density (SMD) [20]. The spin–spin coupling constants were obtained for the most stable conformers of each compound in the gas phase at the same level of theory. The input geometries considered all possible staggered conformations based on the H–O–C–C, O–C–C–N, and C–C–N–H dihedral angles, resulting in a total of 27 theoretical conformers. The optimized geometries, which converged to fewer than 27 distinct conformers, were subjected to NBO analysis [21], including the NBODEL keyword to determine the Lewis- and non-Lewis-type contributions to the electronic energies, as well as specific electron-delocalization interactions responsible for hydrogen bonding, the gauche effect, and other effects. The Lewis (E_L) and non-Lewis (E_{NL}) energy contributions were obtained from the NBO deletion analysis. For comparison of the conformers, the conformation with the lowest E_{NL} contribution was chosen as the reference and assigned an E_{NL} value of zero. The E_{NL} values reported for the other conformers therefore represent

their differences relative to this reference, with negative values indicating more stabilizing non-Lewis interactions than in the reference conformation. The corresponding E_L values were defined with the opposite sign, such that the Lewis and non-Lewis contributions sum to zero for each conformational energy difference. Consequently, the absolute values reported for E_L and E_{NL} depend on the choice of reference conformation, whereas the differences between conformers and the resulting interpretation are independent of this choice. For the complexes, a Zn^{2+} ion was positioned near the nitrogen lone pair electrons of either **1** or **2**, followed by optimization and frequency calculations in the gas phase. Calculations were performed only for Zn^{2+}, since the treatment of Cd^{2+} requires a pseudopotential and would prevent a direct comparison with Zn^{2+} at the same level of theory; the conclusions for Cd^{2+} therefore rely on the experimental $^3J_{H1,H2}$ values and are inferred by analogy with Zn^{2+}. The calculations were all performed in the Gaussian16 suite [22].

Results and Discussion

Given that both **1** and **2** have three rotational bonds, each with three staggered orientations, a total of 27 (3^3) conformers is theoretically possible (Figure 2). However, optimization in the gas phase resulted in 23 distinct conformers for **1** and 18 for **2**. In implicit acetonitrile, where intramolecular dipolar interactions are reduced, all conformers of **1** were obtained, whereas 21 distinct conformers were observed for **2**. Despite the extensive diversity of conformers, only a few exist in significant amounts in the gas phase, specifically *g3* and *g17*, at 58% and 20%, respectively (Table 1). These percentages decrease to 37% and

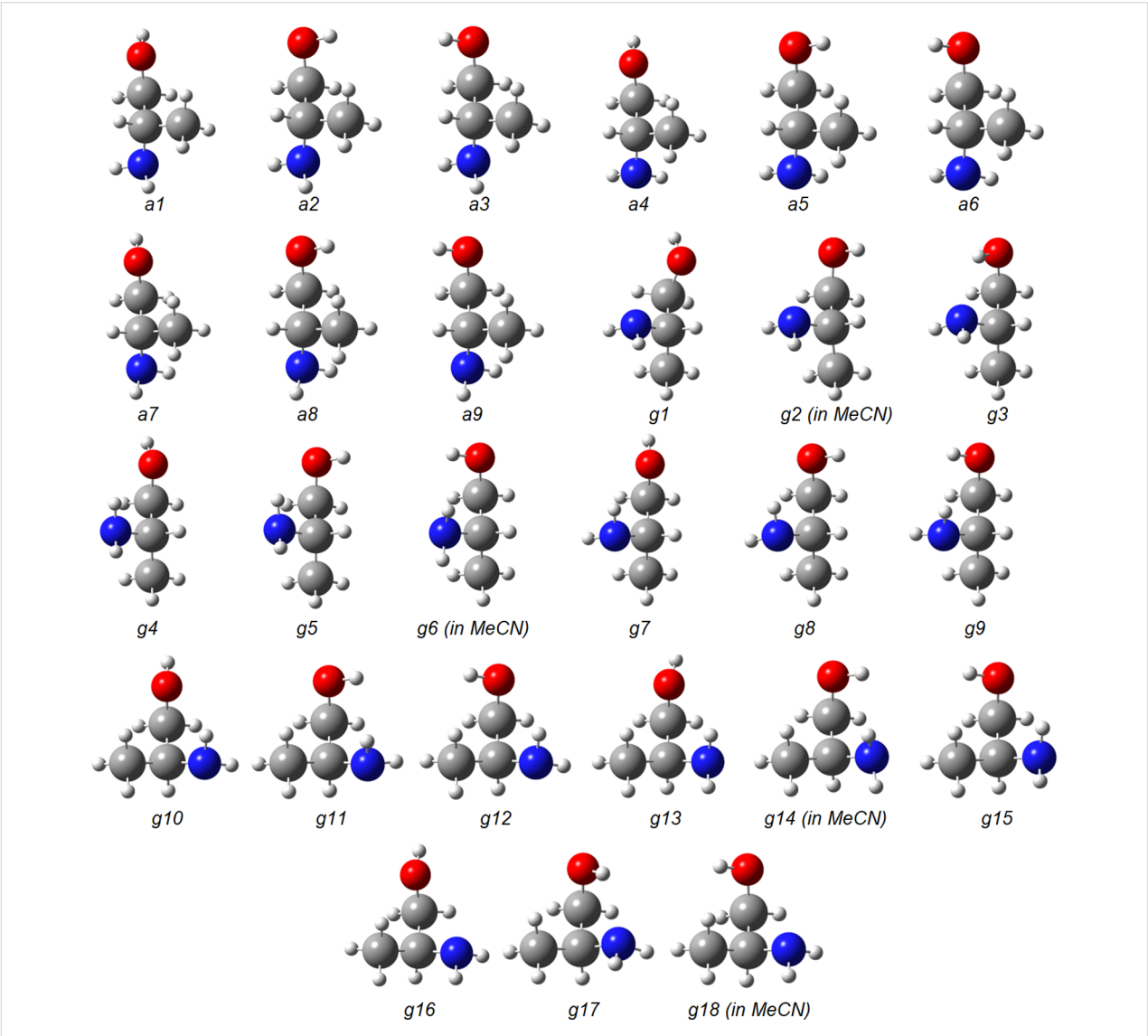


Figure 2: Conformers of **1** with geometries optimized at the B3LYP-GD3BJ/6-311++G(d,p) level.

Table 1: Relative Gibbs free energies ($\Delta G°$, kcal mol^{-1}), conformer populations (p, %), and dipole moments (μ, Debye) for the conformers of **1** and **2** in the gas phase and implicit MeCN.

Conformer	**1**		**2**	
	$\Delta G°_{gas}$ (p) [μ]	$\Delta G°_{MeCN}$ (p) [μ]	$\Delta G°_{gas}$ (p) [μ]	$\Delta G°_{MeCN}$ (p) [μ]
a1	2.61 (1) [0.96]	2.09 (1) [1.52]	1.13 (5) [0.88]	0.75 (7) [1.44]
a2	2.80 (1) [1.67]	1.83 (2) [2.14]		
a3	2.79 (1) [2.70]	1.92 (1) [3.71]	2.21 (1) [2.40]	1.67 (1) [3.56]
a4	2.66 (1) [2.56]	1.80 (2) [3.55]	1.14 (5) [2.23]	0.65 (8) [3.27]
a5	2.76 (1) [1.48]	1.62 (2) [2.03]		
a6	2.76 (1) [1.35]	1.64 (2) [1.84]	2.15 (1) [1.29]	1.43 (2) [1.86]
a7	2.69 (1) [1.02]	2.14 (1) [1.68]	1.21 (4) [0.90]	0.99 (5) [1.53]
a8	3.11 (0) [2.82]	1.98 (1) [3.82]		
a9	2.85 (0) [1.63]	1.98 (1) [2.23]	2.23 (1) [1.39]	1.78 (1) [1.99]
g1	4.50 (0) [2.33]	2.69 (0) [3.68]	3.17 (0) [2.05]	1.48 (2) [3.30]
g2		2.22 (1) [3.87]	3.34 (0) [1.93]	1.98 (1) [3.34]
g3	0.00 (58) [3.33]	0.00 (37) [4.30]	3.05 (0) [2.29]	2.65 (0) [3.25]
g4	1.50 (5) [1.03]	1.25 (5) [1.64]	0.00 (34) [1.02]	0.08 (22) [1.67]
g5	1.86 (2) [2.56]	1.13 (6) [3.71]	1.26 (4) [2.34]	0.86 (6) [3.57]
g6		1.30 (4) [2.20]		
g7	1.71 (3) [2.69]	1.26 (4) [3.73]	0.19 (25) [2.39]	0.00 (25) [3.46]
g8	1.91 (2) [1.57]	1.14 (5) [2.08]	1.32 (4) [1.46]	0.80 (6) [2.02]
g9	2.26 (1) [1.44]	1.15 (5) [1.88]		
g10	2.49 (1) [2.69]	2.14 (1) [3.65]	0.92 (7) [2.40]	0.79 (7) [3.37]
g11	2.81 (1) [1.28]	1.80 (2) [1.72]		
g12	2.54 (1) [1.51]	1.77 (2) [2.02]		2.33 (0) [2.86]
g13	2.35 (1) [1.08]	2.19 (1) [1.70]	0.80 (9) [1.08]	0.94 (5) [1.70]
g14		1.99 (1) [2.35]		3.52 (0) [1.81]
g15	2.76 (1) [2.64]	1.94 (1) [3.76]		2.37 (0) [3.27]
g16	4.78 (0) [2.44]	3.30 (0) [3.76]	3.27 (0) [2.07]	2.02 (1) [3.38]
g17	0.63 (20) [3.14]	0.82 (9) [4.16]	3.00 (0) [2.19]	2.80 (0) [3.17]
g18		2.67 (0) [3.81]	5.41 (0) [1.51]	3.50 (0) [3.52]

9% in implicit acetonitrile, respectively, but conformers *g3* and *g17* remain the most stable. Consistent with a hydrogen-bond rationale, *g3* and *g17* exhibit the OH hydrogen directed towards the nitrogen electron lone pair. In contrast, conformers with a N–H bond nearly oriented towards an oxygen lone pair (*g4*, *g5*, *g7*, *g8*, *g10*, *g12*, *g13*, and *g15*) are negligibly populated, ranging from 0% to 5%, with no $n_O \rightarrow \sigma^*_{NH}$ appearing in the NBO outcomes. Clearly, the N···H–O interaction determines the conformational equilibrium of 1, similar to 2-amino-2-methylpropanol, where the hydrogen-bonded conformation is populated by approximately 78% in the gas phase [1]. Nevertheless, secondary effects contribute to the higher stability of *gauche* conformers compared to *anti* conformers. All nine *anti* conformers have relative energies above 2.6 kcal mol^{-1}, whereas only three out of thirteen *gauche* conformers exceed this energy threshold owing to clashing interactions such as NH···HO, CH···HO, or $n_O \cdots n_N$. This higher stability is often referred to as the gauche effect, an anomalous behavior attributed to stabilizing antiperiplanar electron delocalization between good electron donors (σ_{CH} or σ_{CC}) and good electron acceptors (σ^*_{CO} and σ^*_{CN}), which is inactive in the *anti* conformation. While the aforementioned hydrogen bond and gauche effect can be confirmed by the hyperconjugative interactions depicted in Table 2 and obtained from NBO analysis, the Lewis (E_L) and non-Lewis (E_{NL}) contributions to the total electronic energy of each system provide insights into the overall repulsive and electron-delocalization effects that govern the conformational equilibrium of **1**. From this analysis, *g11* is the most disfavored conformer in terms of E_L, while *g4* is the least disfavored by this metric. Conversely, *g9* is the most favored conformer in terms of E_{NL}, while *a1* is the least favored. Notably, conformer *g3* is significantly favored by a non-Lewis (E_{NL}) contribution of 8.00 kcal mol^{-1}, which is consistent with the presence of a N···H–O hydrogen bond (Figure 3). NBO second-order pertur-

Table 2: Lewis- (E_L) and non-Lewis (E_{NL}) contributions for the relative electronic energies (E) of the conformers of **1**, as well as the relevant interactions for hydrogen bonding and the gauche effect (kcal mol^{-1}).

Conformer	E	E_L	E_{NL}	n_N/σ^*_{OH}	$\sigma_{CH}/\sigma^*_{CO}$	$\sigma_{CC}/\sigma^*_{CO}$	$\sigma_{CH}/\sigma^*_{CN}$	$\sigma_{CO}/\sigma^*_{CN}$	$\sigma_{CN}/\sigma^*_{CO}$
a1	3.33	3.33	0.00					1.69	2.01
a2	3.42	6.02	−2.60					1.39	2.22
a3	3.37	6.84	−3.46					1.43	2.15
a4	3.42	8.01	−4.59					1.89	1.7
a5	3.36	10.58	−7.22					1.56	1.93
a6	3.34	10.47	−7.13					1.6	1.88
a7	3.49	6.25	−2.76					1.69	2.14
a8	3.78	9.81	−6.03					1.37	2.33
a9	3.51	8.58	−5.07					1.42	2.29
g1	6.05	10.97	−4.92			2.23	3.5		
g3	0.00	8.00	−8.00	2.97		2.18	3.43		
g4	1.93	2.72	−0.79			2.42	3.46		
g5	2.17	6.17	−4.01			2.73	3.4		
g7	2.29	7.26	−4.97			2.33	4.08		
g8	2.34	8.86	−6.51			2.64	4.02		
g9	2.90	11.04	−8.15			2.74	4.34		
g10	3.08	6.91	−3.83		4.27		4.19		
g11	3.32	11.21	−7.89		4.78		4.4		
g12	2.96	9.05	−6.09		4.69		4.1		
g13	2.79	5.18	−2.40		4.39		3.53		
g14	3.07	8.91	−5.85		4.84		3.42		
g16	5.96	9.67	−3.71		4.52		3.9		
g17	0.54	4.93	−4.39	2.45	3.96		3.41		

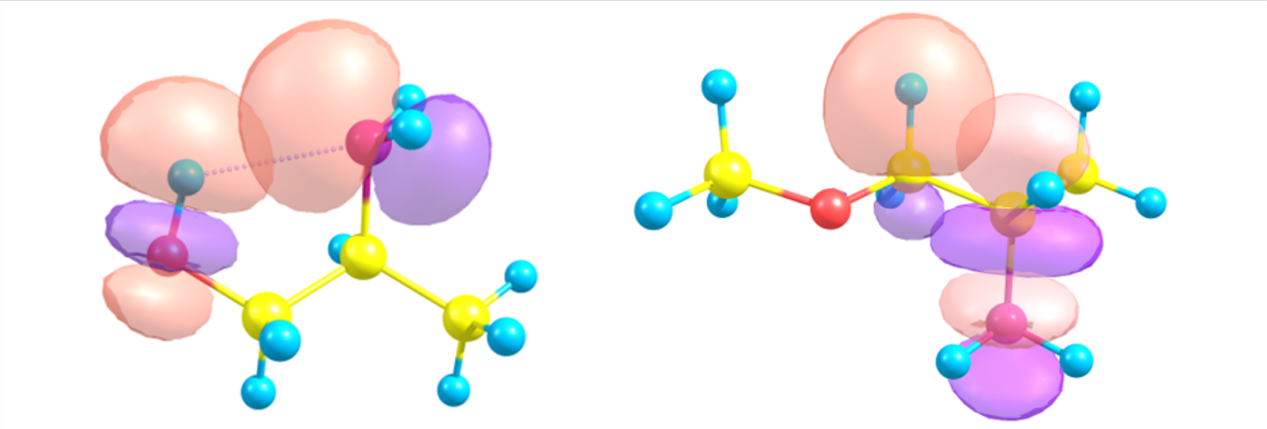


Figure 3: NBO plots illustrating the intramolecular hydrogen-bonding interaction in **1** *g3* ($n_N \rightarrow \sigma^*_{OH}$) and the electron delocalization in **2** ($\sigma_{CH} \rightarrow \sigma^*_{CN}$) that contributes to stabilization of the *g4* conformer.

bation analysis estimates the associated $n_N \rightarrow \sigma^*_{O-H}$ donor–acceptor stabilization at 2.97 kcal mol^{-1}. This value should be regarded only as a qualitative indication of the relative importance of the interaction, not as a precise hydrogen-bond strength. In contrast, in the Zn^{2+} complex, NBO analysis describes the Zn–N and Zn–O interactions as formal bonds (with bond occupancies of 1.9556 and 1.9747, respectively), so they are not treated as donor–acceptor interactions and no second-order perturbation energy is associated with them. Given the electrostatic and charge-transfer character of these dication–ligand contacts, they are expected to be considerably stronger than the N···H–O hydrogen bond. Overall, the stability of the conformers is governed by a balance between Lewis (E_L) and non-Lewis (E_{NL}) contributions.

To gain further insights into the strength of the intramolecular hydrogen bond in **1**, the methyl ether derivative **2** was comprehensively investigated (Figure 4). Unlike **1**, derivative **2** cannot exhibit a N···H–O hydrogen bond and can only form an O···H–N hydrogen bond. Consequently, conformers *g3* and *g17* of compound **2**, which were prevalent forms in compound **1**, exhibit high energy and are negligibly populated. Instead, conformers *g4*, *g7*, *g10*, and *g13* of **2**, with relative energies less than 1 kcal mol^{-1} in both the gas phase and implicit acetonitrile, are significantly populated (Table 1). In these conformers, the

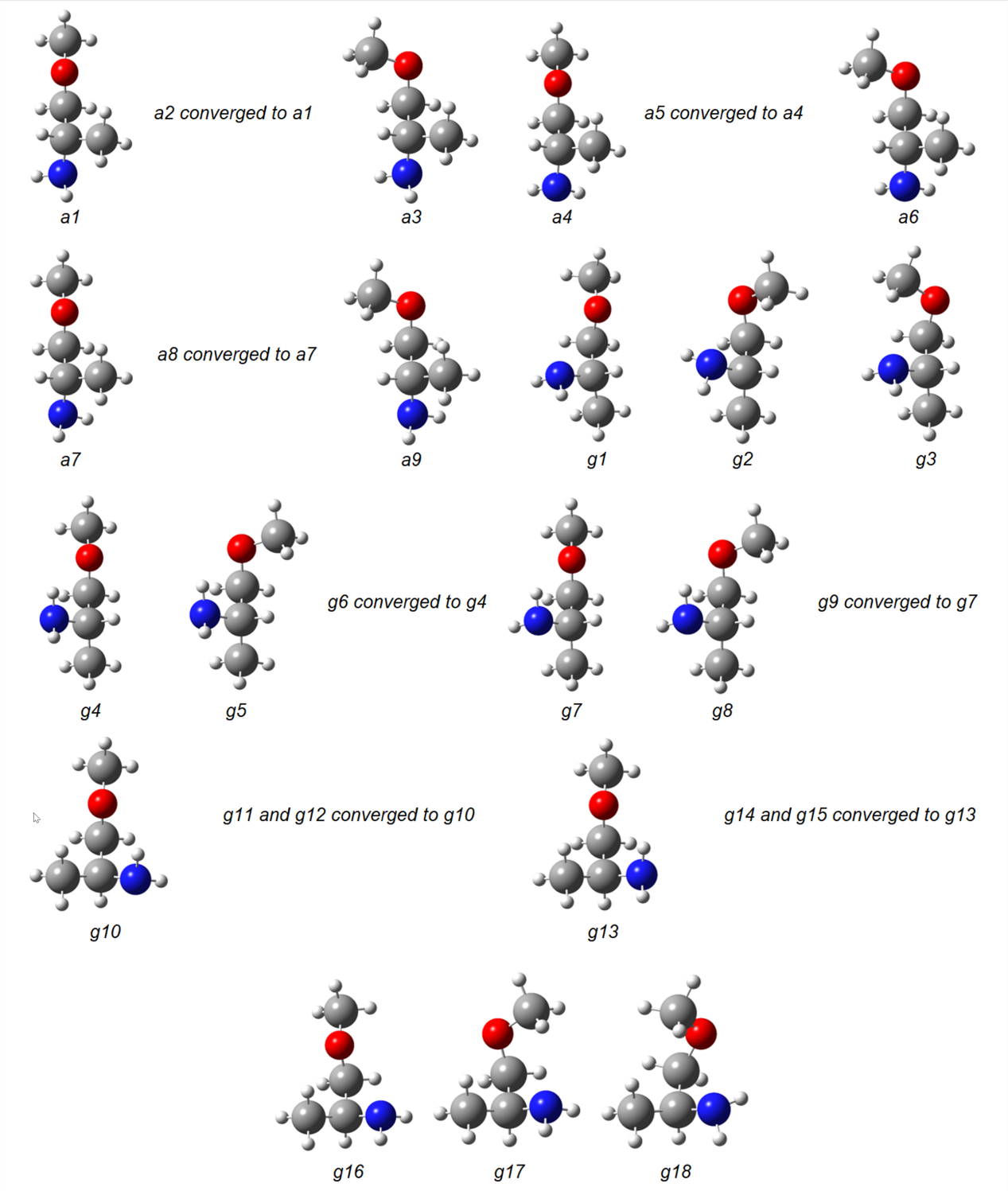


Figure 4: Conformers of **2** with geometries optimized at the B3LYP-GD3BJ/6-311++G(d,p) level.

methoxy (OMe) group is antiperiplanar to the central C–C bond to relieve steric hindrance, while an N–H hydrogen is directed towards an oxygen electron lone pair. However, no $n_O \rightarrow \sigma_{NH}$ interaction was observed in the NBO analysis. The general preference for *gauche* conformers over *anti* conformers in compound **2** suggests that the gauche effect, due to hyperconjugative interactions such as $\sigma_{CH} \rightarrow \sigma^*_{CO}$, $\sigma_{CC} \rightarrow \sigma^*_{CO}$, and $\sigma_{CH} \rightarrow \sigma^*_{CN}$ (Table 3), reinforced by weak steric effects, governs the conformational equilibrium of compound **2**. Indeed, the conformer *g1* is the most favored according to E_{NL}, while conformer *g4* is the least disfavored according to E_L.

An atoms in molecules (AIM) analysis reinforced the NBO findings, as the *g3* and *g17* conformers of **1** exhibited a bond path between N and H(O), indicating the formation of a hydrogen bond (Figure 5). In contrast, the remaining conformers possessing a N–H bond directed towards the oxygen in either **1** or **2** do not show bond paths suggesting the presence of a hydrogen bond. Notably, the electron densities at the bond critical point of the *g3* and *g17* conformers of **1** are 0.0205 and 0.0191, respectively, indicating that the former engages in a stronger interaction.

The *gauche* preference for the N–C–C–O fragment is observed in both compounds **1** and **2**, but for different reasons (hydrogen bonding or the gauche effect) and to varying extents (more favored in **1**). This theoretical finding is supported by NMR spin–spin coupling constants (SSCCs) between H-2 and the diastereotopic hydrogens at C-1. While a large $^3J_{H1,H2}$ and a small $^3J_{H1,H2}$ are anticipated for *anti* conformers and for *g1* to *g8* (due to one *gauche* and one antiperiplanar arrangement of H1–C–C–H2), two small $^3J_{H1,H2}$ values are expected for *g10* to *g18* conformers. Considering the calculated $^3J_{H1,H2}$ values for the main *anti* and *gauche* conformers of **1** and **2** shown in Table 4, along with the experimental measurements, we conclude that *anti* and *g1–g8* conformers are highly prevalent in both $CDCl_3$ and CD_3CN solutions, rather than *g10–g18*. Assuming that *anti* conformers contribute only a minor proportion to the conformational populations, and that *g3* for **1**, and *g4* and *g7* for **2** are calculated to be predominant, the observed SSCCs are mainly due to these latter conformers. However, it is noteworthy that as the $^3J_{H1,H2}$ values vary from $CDCl_3$ to CD_3CN

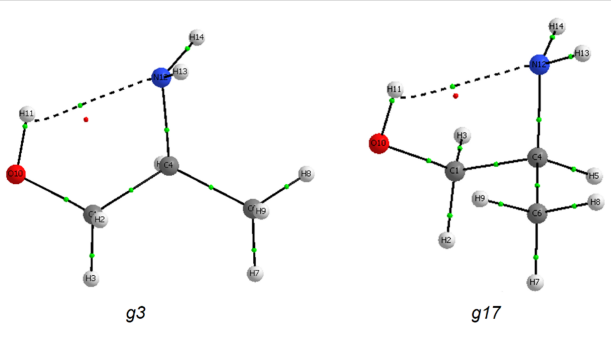


Figure 5: Conformers of **1** exhibiting a bond path between N and H(O). The electron densities (ρ) at the bond critical point of *g3* and *g4* are 0.0205 and 0.0191, respectively, according to AIM calculations.

Table 3: Lewis- (E_L) and non-Lewis (E_{NL}) contributions for the relative electronic energies (E) of the conformers of **2**, as well as the relevant interactions for the gauche effect (kcal mol^{-1}).

Conformer	E	E_L	E_{NL}	$\sigma_{CH}/\sigma^*_{CO}$	$\sigma_{CC}/\sigma^*_{CO}$	$\sigma_{CH}/\sigma^*_{CN}$	$\sigma_{CO}/\sigma^*_{CN}$	$\sigma_{CN}/\sigma^*_{CO}$
a1	1.38	1.76	–0.38				1.55	1.98
a3	2.60	3.99	–1.39				1.22	2.31
a4	1.41	5.87	–4.47				1.74	1.67
a6	2.40	7.46	–5.05				1.33	2.01
a7	1.52	4.54	–3.02				1.55	2.1
a9	2.44	6.24	–3.80				1.16	2.4
g1	3.91	10.06	–6.15		2.2	3.48		
g2	3.54	9.09	–5.56		2.9	3.66		
g3	3.27	7.48	–4.22		2.61	3.78		
g4	0.00	0.90	–0.90		2.33	3.41		
g5	1.28	3.83	–2.56		2.81	3.3		
g7	0.34	5.29	–4.95		2.26	4.03		
g8	1.45	5.81	–4.36		2.7	3.89		
g10	1.04	5.11	–4.07	4.08		4.13		
g13	0.77	3.38	–2.61	4.17		3.47		
g16	3.74	8.44	–4.70	4.34		3.83		
g17	3.02	5.73	–2.71	4.72		4.03		
g18	5.33	5.33	0.00	3.79		2.99		

(as shown in Table 4), the conformational populations also change, leading to an increased proportion of *g10*–*g18* in CD_3CN.

The extension of the intramolecular hydrogen bond can be probed by infrared spectroscopy, as bonds involved in such interactions are weakened, leading to a reduction in the corresponding vibration wavenumber. Notably, the calculated stretching mode for the O–H bond in *g3* and *g17* of compound **1** is red-shifted by more than 100 cm^{-1} compared to the other conformers (Table 5), indicating that the N···H–O hydrogen bond strongly affects these two conformers. Conversely, the symmetric and asymmetric stretching modes of the NH_2 group exhibit only a subtle decrease in wavenumbers for conformers *g7*, *g8*, *g10*, and *g12*, suggesting that any O···H–N hydrogen bond present is fragile. This same behavior is observed in compound **2**. Experimentally, compound **1** exhibited two sets of convoluted bands in the O–H stretching region in $CHCl_3$ and CH_3CN solutions (0.05 M). The more red-shifted set of bands (centered at approximately 3629 cm^{-1} in $CHCl_3$ and 3529.2 cm^{-1} in CH_3CN), corresponding to the *g3* and *g17* conformers, were more intense than the blue-shifted bands (centered at 3668 cm^{-1} in $CHCl_3$ and 3629 cm^{-1} in CH_3CN) associated with the remaining conformers. After band deconvolution (Figure 6), the

Table 4: Calculated and experimental spin–spin coupling constants (in Hz) for **1**, **2**, and the metallic complexes.

Conformer	**1**		**2**	
	$^3J_{H1a,H2}$	$^3J_{H1b,H2}$	$^3J_{H1a,H2}$	$^3J_{H1b,H2}$
a1			7.7	3.2
a4			8.3	3.6
a7			8.8	4.1
g3	8.5	3.8		
g4			8.0	2.4
g7			8.2	2.7
g10			14.5	2.7
g13			2.2	2.6
g17	3.0	1.0		
g-Zn^{2+} (0.0 kcal mol^{-1})	9.6	4.9	9.5	4.8
g-Zn^{2+} (0.7 kcal mol^{-1})	3.4	0.8	2.4	0.9
exp. ($CDCl_3$)	7.8	4.0	8.0	3.9
exp. (CD_3CN)	7.3	4.6	7.3	4.8
exp. $ZnCl_2$ (CD_3CN)	8.3	3.9	8.6	3.6
exp. $CdCl_2$ (CD_3CN)	7.6	4.3	8.5	3.7

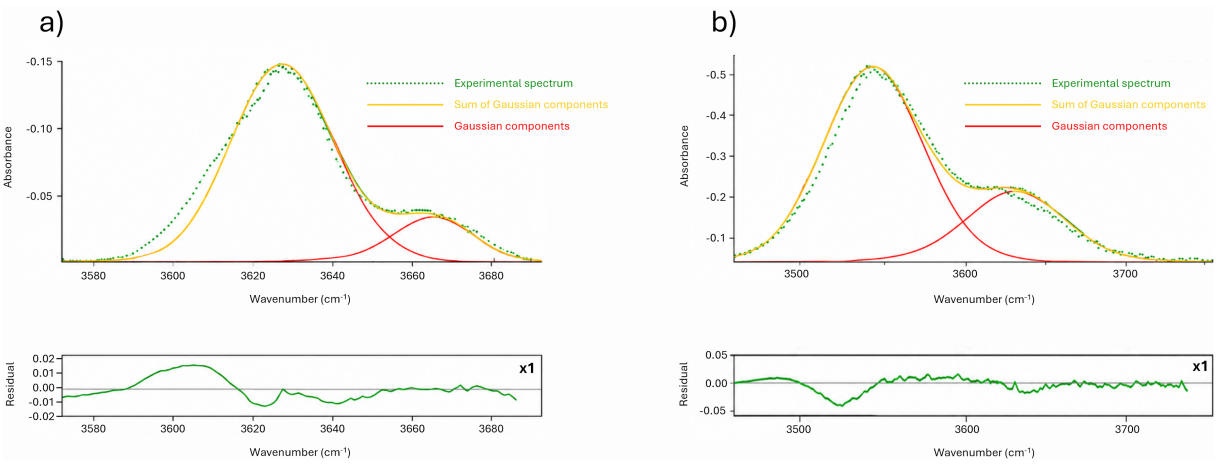


Figure 6: O–H stretching bands of compound **1** (2-aminopropan-1-ol) in 0.05 M solutions of (a) chloroform ($CHCl_3$) and (b) acetonitrile (CH_3CN). Upper plots show the absorbance spectra; red curves represent the Gaussian components used to deconvolute the yellow overall fits. Lower plots show the corresponding residuals between the experimental spectra (dotted green lines) and the fitted curves (solid yellow lines) in the upper plots.

Table 5: Calculated frequencies (cm^{-1}) for O–H and NH_2 stretching modes in **1** and **2**, obtained at the B3LYP-GD3BJ/6-311++G(d,p) level.

Conformer	**1**			**2**	
	ν(OH)	$\nu(NH_2)_{as}$	$\nu(NH_2)_{sym}$	$\nu(NH_2)_{as}$	$\nu(NH_2)_{sym}$
a1	3857.3	3580.9	3501.8	3589.4	3501.4
a2	3843.7	3579.4	3501.1		
a3	3829.4	3582.9	3503.1	3579.2	3500.0
a4	3849.8	3573.4	3489.8	3572.1	3489.0
a5	3842.0	3571.1	3488.0		
a6	3829.2	3570.9	3488.5	3568.4	3485.4
a7	3855.7	3574.2	3490.8	3573.2	3490.0
a8	3842.6	3575.6	3492.3		
a9	3834.4	3570.2	3488.6	3571.2	3488.6
g1	3856.1	3575.7	3488.8	3573.4	3487.6
g2	3819.5[a]	3541.0[a]	3466.5[a]	3585.9	3501.9
g3	3716.5	3582.0	3492.8	3561.2	3479.0
g4	3857.7	3581.8	3502.9	3582.2	3502.8
g5	3827.9	3585.5	3504.6	3584.7	3503.2
g6	3825.9[a]	3554.6[a]	3488.7[a]		
g7	3856.0	3566.7	3482.9	3565.6	3482.2
g8	3828.0	3559.6	3481.0	3556.4	3478.5
g9	3828.1	3589.0	3493.7		
g10	3860.0	3566.9	3489.7	3566.1	3488.9
g11	3824.8	3585.9	3496.5		
g12	3839.7	3562.8	3486.3	3538.3[a]	3467.9[a]
g13	3863.0	3575.8	3496.8	3576.1	3497.0
g14	3820.3[a]	3548.0[a]	3477.2[a]	3551.7[a]	3484.6[a]
g15	3841.2	3578.4	3497.3	3543.7[a]	3473.4[a]
g16	3856.9	3582.4	3501.1	3581.9	3500.7
g17	3726.6	3586.9	3505.9	3571.4	3492.8
g18	3826.5[a]	3554.0[a]	3482.1[a]	3598.7	3512.9

[a]In implicit MeCN solution.

relative intensities of the bands indicated that *g3* and *g17* conformers are populated by 82% and 74% in $CHCl_3$ and CH_3CN solutions, respectively, which is qualitatively in line with calculations. A similar analysis for compound **2** could not be performed due to the absence of an O–H group and distinguishable bands.

The N···H–O hydrogen bond in compound **1** is sufficiently strong to control its conformational equilibrium, whereas the gauche effect in compound **2** plays a pivotal role in determining its conformational preferences. The O···H–N hydrogen bond does not appear to influence the conformational stability of either compound **1** or **2**. While these interactions modulate the conformational equilibrium of the studied compounds, could they prevent chelation with metallic ions, thus hindering the effective removal of heavy metals from soil and water? To address this question, a Zn^{2+} ion was theoretically positioned near the nitrogen atom of all conformers of compounds **1** and **2**. As a result, only two low-energy structures were found where the metallic ion chelated with both nitrogen and oxygen forming a bidentate complex (Figure 7), resembling a *gauche* conformation with the N–H and O–R (R = H and Me) bonds directed opposite the cation. The other structures exhibited very high energy in the gas phase (greater than 25 kcal mol^{-1}), indicating that the metallic interaction is strong enough to disrupt the intramolecular hydrogen bond. However, the bidentate arrangement is disrupted in implicit acetonitrile, and the corresponding structure is no longer the most stable.

To experimentally verify these findings, the SSCCs for the complexes of compounds **1** and **2** with $ZnCl_2$ and $CdCl_2$ in saturated CD_3CN were measured. The results showed one large and one small $^3J_{H1,H2}$ coupling constant (Table 4), confirming the prevalence of the complexes with such arrangements (one

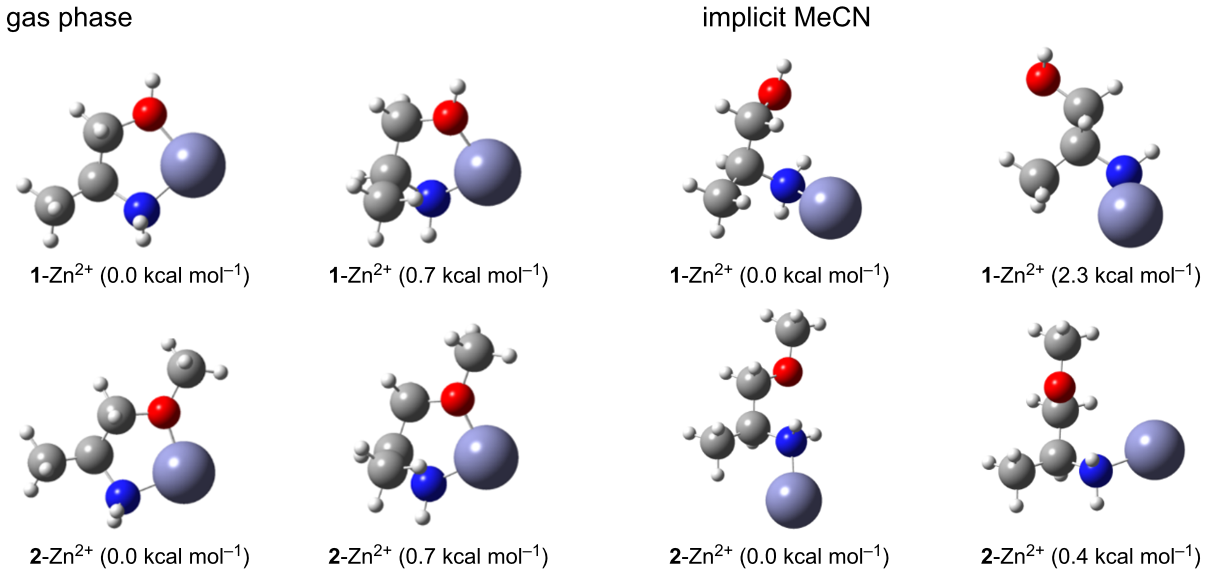


Figure 7: Most stable geometry-optimized complexes formed between Zn^{2+} and compounds **1** and **2** in the gas phase and implicit acetonitrile. The bidentate structures in the gas phase are disrupted, resulting in open structures as the main conformations in implicit acetonitrile.

antiperiplanar and one *gauche* H1–C–C–H2). However, it appears that the complex of compound **1** with Cd^{2+} has a greater contribution from structures with both H1–C–C–H2 dihedral angles in a *gauche* arrangement, as the $^3J_{H1,H2}$ values are 7.6 and 4.3 Hz, rather than the values above 8.0 and below 4.0 Hz observed for the other complexes. This difference may reflect the effects of the solvent and the chloride counterions, which are not explicitly included in the gas-phase model, and should be interpreted with caution given the small magnitude of the deviation. Cadmium has two spin-$^1/_2$ isotopes (^{111}Cd and ^{113}Cd), and scalar couplings between Cd and nuclei in non-bonded contacts have been observed when a suitable through-space or hydrogen-bond-mediated pathway exists [14,23]. We therefore searched for an (O)H···Cd coupling, either directly or through satellite peaks, but none was detected. This may reflect an inefficient coupling pathway and/or rapid exchange in solution. Consequently, the NMR data neither support nor exclude an (O)H···Cd interaction.

Conclusion

The conformational equilibrium of 2-aminopropan-1-ol is primarily governed by an intramolecular hydrogen bond, with nitrogen acting as the hydrogen-bond acceptor and the OH group as the donor. In the methyl ether derivative, where this hydrogen bond is not possible, the conformational balance is determined by the gauche effect arising from antiperiplanar hyperconjugative interactions. However, calculations for the Zn^{2+} complexes, together with the experimental $^3J_{H1,H2}$ coupling constants measured for both Zn^{2+} and Cd^{2+} complexes, show that these intramolecular interactions do not prevent chelation: the cation coordination overrides the conformational preferences of the free compounds. Computational results are available only for Zn^{2+}, and the behavior of Cd^{2+} is inferred from the similarity of the experimental coupling constants, with the exception of the Cd^{2+} complex of **1**, whose small deviation may reflect solvent and counterion effects not explicitly included in the model. These findings suggest that the intramolecular interactions in these compounds are not strong enough to prevent chelation of divalent cations in environments such as enzymes, soil, and water, although specific intermolecular interactions with polar solvents may disfavor chelation.

Supporting Information

Supporting Information File 1

^{1}H NMR spectra of **1**, **2**, and their complexes with $ZnCl_2$ and $CdCl_2$ and standard coordinates of the conformers of **1**, **2**, and their complexes with Zn^{2+}.
[https://www.beilstein-journals.org/bjoc/content/supplementary/1860-5397-22-133-S1.pdf]

Acknowledgements

We also gratefully acknowledge Professor Rodrigo A. Cormanich for his support in acquiring the NMR spectra.

Funding

The authors are thankful to Coordenação de Aperfeiçoamento de Pessoal de Nível Superior (CAPES, funding code 001) and

Conselho Nacional de Desenvolvimento Científico e Tecnológico (CNPq, grant number 317093/2025-8) for financial support of this research.

Author Contributions

Lauane C. Mendonça: investigation; writing – review & editing. Matheus P. Freitas: conceptualization; formal analysis; funding acquisition; methodology; supervision; writing – original draft.

ORCID® iDs

Matheus P. Freitas - https://orcid.org/0000-0002-7492-1801

Data Availability Statement

All data that supports the findings of this study is available in the published article and/or the supporting information of this article.

References

1. Andrade, L. A. F.; Silla, J. M.; Freitas, M. P. *J. Mol. Struct.* **2014,** *1072,* 203–207. doi:10.1016/j.molstruc.2014.05.006
2. Lämmermann, A.; Szatmári, I.; Fülöp, F.; Kleinpeter, E. *J. Phys. Chem. A* **2009,** *113,* 6197–6205. doi:10.1021/jp902731n
3. Gonçalves, K. M. S.; Garcia, D. R.; Ramalho, T. C.; Figueroa-Villar, J. D.; Freitas, M. P. *J. Phys. Chem. A* **2013,** *117,* 10980–10984. doi:10.1021/jp408528j
4. Hartwig, B.; Schnell, M.; Suhm, M. A.; Obenchain, D. A. *Phys. Chem. Chem. Phys.* **2024,** *26,* 9432–9452. doi:10.1039/d3cp04911f
5. Martins, F. A.; Ramalho, T. C.; Freitas, M. P. *Spectrochim. Acta, Part A* **2023,** *288,* 122205. doi:10.1016/j.saa.2022.122205
6. Silva, C. F. P.; Duarte, M. L. T. S.; Fausto, R. *J. Mol. Struct.* **1999,** *482-483,* 591–599. doi:10.1016/s0022-2860(98)00794-7
7. Liu, Y.; Rice, C. A.; Suhm, M. A. *Can. J. Chem.* **2004,** *82,* 1006–1012. doi:10.1139/v04-046
8. Thomsen, D. L.; Axson, J. L.; Schrøder, S. D.; Lane, J. R.; Vaida, V.; Kjaergaard, H. G. *J. Phys. Chem. A* **2013,** *117,* 10260–10273. doi:10.1021/jp405512y
9. Lane, J. R.; Schrøder, S. D.; Saunders, G. C.; Kjaergaard, H. G. *J. Phys. Chem. A* **2016,** *120,* 6371–6378. doi:10.1021/acs.jpca.6b05898
10. Lwin, E.; Gölz, M. J.; Lüttschwager, N. O. B.; Suhm, M. A.; Käser, S.; Andreichev, V.; Brandes, M. A.; Meuwly, M. *Phys. Chem. Chem. Phys.* **2025,** *27,* 17692–17703. doi:10.1039/d5cp02019k
11. Guimarães, M. C.; Silla, J. M.; da Cunha, E. F. F.; Ramalho, T. C.; Freitas, M. P. *RSC Adv.* **2016,** *6,* 111681–111687. doi:10.1039/c6ra23423b
12. Armesto, N.; Fernández, S.; Ferrero, M.; Gotor, V. *Tetrahedron* **2006,** *62,* 5401–5410. doi:10.1016/j.tet.2006.03.074
13. McCall, K. A.; Huang, C.-c.; Fierke, C. A. *J. Nutr.* **2000,** *130,* 1437S–1446S. doi:10.1093/jn/130.5.1437s
14. Silva, V. L.; Carvalho, R.; Freitas, M. P.; Tormena, C. F.; Melo, W. C. *Spectrochim. Acta, Part A* **2007,** *68,* 1197–1200. doi:10.1016/j.saa.2007.01.020
15. Carvalho, A. V. S.; Carvalho, R.; Abreu, C. M. P.; Furtini Neto, A. E.; Freitas, M. P. *Commun. Soil Sci. Plant Anal.* **2009,** *40,* 2959–2974. doi:10.1080/00103620903261296
16. Becke, A. D. *J. Chem. Phys.* **1993,** *98,* 5648–5652. doi:10.1063/1.464913
17. Lee, C.; Yang, W.; Parr, R. G. *Phys. Rev. B* **1988,** *37,* 785–789. doi:10.1103/physrevb.37.785
18. Grimme, S.; Ehrlich, S.; Goerigk, L. *J. Comput. Chem.* **2011,** *32,* 1456–1465. doi:10.1002/jcc.21759
19. Krishnan, R.; Binkley, J. S.; Seeger, R.; Pople, J. A. *J. Chem. Phys.* **1980,** *72,* 650–654. doi:10.1063/1.438955
20. Marenich, A. V.; Cramer, C. J.; Truhlar, D. G. *J. Phys. Chem. B* **2009,** *113,* 6378–6396. doi:10.1021/jp810292n
21. *NBO 7.0;* Theoretical Chemistry Institute, University of Wisconsin: Madison, 2018.
22. *Gaussian 16,* Revision C.01; Gaussian, Inc.: Wallingford, CT, 2016.
23. Loening, N. M.; Anderson, C. E.; Iskenderian, W. S.; Anderson, C. D.; Rychnovsky, S. D.; Barfield, M.; O'Leary, D. J. *Org. Lett.* **2006,** *8,* 5321–5323. doi:10.1021/ol062121v

License and Terms

This is an open access article licensed under the terms of the Beilstein-Institut Open Access License Agreement (https://www.beilstein-journals.org/bjoc/terms), which is identical to the Creative Commons Attribution 4.0 International License (https://creativecommons.org/licenses/by/4.0). The reuse of material under this license requires that the author(s), source and license are credited. Third-party material in this article could be subject to other licenses (typically indicated in the credit line), and in this case, users are required to obtain permission from the license holder to reuse the material.

The definitive version of this article is the electronic one which can be found at:
https://doi.org/10.3762/bjoc.22.133